Corrosion Science 168 (2020) 108566

Contents lists available at ScienceDirect

Corrosion Science

journal homepage: www.elsevier.com/locate/corsci

Surface modified Ti6Al4V for enhanced bone bonding ability – Effects of silver and corrosivity at simulated physiological conditions from a corrosion and metal release perspective

Yolanda S. Hedberg[a,*], Francesca Gamna[a,b], Gianmaria Padoan[a,b], Sara Ferraris[b], Martina Cazzola[b], Gunilla Herting[a], Masoud Atapour[a,c], Silvia Spriano[b,1], Inger Odnevall Wallinder[a,1]

[a] KTH Royal Institute of Technology, Department of Chemistry, Division of Surface and Corrosion Science, Drottning Kristinas väg 51, SE-10044, Stockholm, Sweden
[b] Materials Physics and Engineering, Department of Applied Science and Technology, Politecnico di Torino, Corso Duca degli Abruzzi 24, 10129, Torino, Italy
[c] Department of Materials Engineering, Isfahan University of Technology, Isfahan, 84156-83111, Iran

ARTICLE INFO

Keywords:
A. Alloy
A. Titanium
A. Silver
B. XPS
B. Polarization

ABSTRACT

Different surface treatments, with and without silver (Ag), of a Ti6Al4V alloy for increased bone bonding ability were investigated and compared with non-treated surfaces. Studies were conducted at 37 °C in phosphate buffered saline (PBS, pH 7.4) of varying hydrogen peroxide (H_2O_2) and bovine serum albumin (BSA) concentrations. Increased levels of metal release and corrosion were observed in the presence of both H_2O_2 and BSA due to complexation with Ti and Al in the surface oxide, respectively. Ag release was enhanced by the presence of BSA. Galvanic effects by Ag were minor, but possibly observed in the most corrosive environment.

1. Introduction

Silver doped surfaces are of interest for biomedical alloy applications, since silver has a known antimicrobial function against pathogens [1]. Biomedical titanium alloys, such as the titanium-aluminium (6 wt-%)-vanadium (4 wt-%) alloy, denoted Ti6Al4V, are often used for bone applications (e.g. screws in dental implants, or stems in hip/knee prostheses) [2]. Successful osseointegration (tight integration into the bone) and high bone bonding ability are crucial processes for these applications. Multifunctional surface engineering combining antimicrobial properties and bone bonding abilities is increasingly employed to elaborate efficient biomaterial surfaces [1]. The investigated Ti6Al4V surfaces of this study are based on a one-step chemical treatment that has been developed to enhance the bone bonding ability, accomplished by modifying the surface morphology generating pores on the nanoscale and a high density of OH groups. These changes in surface morphology and chemistry improve the ability of the surface to induce apatite precipitation, to enhance the cell response and to passively discourage bacteria adhesion [3,4]. An active antimicrobial action is gained via the addition of silver nanoparticles [5].

When silver is electrically coupled to a biomedical alloy, it might negatively influence the corrosion properties and the extent of metal release. Nanostructured silver coated on a Ti6Al4V alloy has been reported to cause both higher cathodic and anodic currents when exposed in 0.9 % NaCl for 10 days at room temperature compared with a non-coated surface. This was explained by effects of galvanic coupling causing silver ion release [6]. However, to the best of the knowledge of the authors, effects of silver incorporated within porous titanium dioxide-rich surface layers, optimized for enhanced bone bonding ability, have not been reported.

The relevance of corrosion tests of highly passive alloys such as Ti6Al4V in simplified media such as 0.9 % NaCl for more severe physiological conditions such as inflammation and infection has recently been questioned [7–10]. Combined and partially complexation-induced chemical and electrochemical processes have been identified to enhance both corrosion and metal release from Ti6Al4V alloys in the presence of proteins (albumin) and hydrogen peroxide (H_2O_2) [7,8,10]. Although similarities have been observed between metal release results of these in vitro studies and reported Ti6Al4V failures [9,10], these findings might not be directly applicable for surface modified Ti6Al4V alloys with thick and/or porous oxides of enhanced bone bonding ability.

* Corresponding author.
E-mail address: yolanda@kth.se (Y.S. Hedberg).
[1] Shared authorship.

https://doi.org/10.1016/j.corsci.2020.108566
Received 12 November 2019; Received in revised form 17 February 2020; Accepted 26 February 2020
Available online 27 February 2020

Table 1
Composition and pH of physiological solutions.

	PBS	PBS + 40 g/L BSA	PBS + 40 g/L BSA + 10μM H_2O_2	PBS + 30 mM H_2O_2	PBS + 40 g/L BSA + 30 mM H_2O_2[a]	PBS + 30 mM H_2O_2 + 40 g/L BSA[b]
NaCl	8.77	8.77	8.77	8.77	8.77	8.77
Na_2HPO_4	1.28	1.28	1.28	1.28	1.28	1.28
KH_2PO_4	1.36	1.36	1.36	1.36	1.36	1.36
BSA	–	40	40	–	40	40
H_2O_2	–	–	10 μM	30 mM	30 mM	30 mM
pH	pH adjusted to 7.2–7.4 using 50% NaOH					

[a] in the case of the electrochemical measurements, the BSA and H_2O_2 were added after 24 h and 48 h of the 1 week OCP measurements, respectively.
[b] in the case of the electrochemical measurements, the H_2O_2 and BSA were added after 24 h and 48 h of the 1 week OCP measurements, respectively.

The aims of this study were to investigate the influence of galvanic effects of silver of a surface modified Ti6Al4V alloy, and effects of albumin and H_2O_2 on both modified and non-modified surfaces in simulated physiological solutions from a metal release and corrosion perspective.

2. Materials and methods

2.1. Materials and treatment

Three different surfaces of the ASTM B348-10 Grade 5 titanium alloy (6.1 wt% Al, 4.1 wt% V, 0.13 wt% Fe, 0.011 wt% C, 0.01 wt% N, 0.002 wt% H and 0.15 wt% O) were prepared and investigated; mirror-polished (denoted MP), surface-treated for enhanced bone bonding ability (denoted treated) and surface-treated including silver nanoparticles in a combined chemical step (denoted treated-Ag). All specimens were exposed as disks (Ø 10 mm; thickness 2 mm). Specimens of MP were consecutively abraded using SiC grinding papers of different grit size and finally polished to 1 μm using diamond paste. The treated and treated-Ag-surfaces were first ground using SiC grit 400 and rinsed with acetone and ultrasonically cleaned with ultrapure water (resistivity:18.2 MΩcm) twice for 5 and 10 min, respectively, followed by acid etching in diluted hydrofluoric acid (HF) at room temperature for 45 min, and a controlled oxidation process in H_2O_2 for 1.5 h (thermostatic bath-Julabo SW23, 60 °C, 120 r.p.m) following a patented chemical treatment procedure [11]. The treated-Ag-specimens followed the same diluted HF (45 min) and controlled oxidation process (H_2O_2) for 45 min, after which $AgNO_3$ (final concentration 0.001 M, PA-ACS-ISO 131459,1611, Panreac), gallic acid (GA, final concentration 0.1 g/L) and polyvinyl alcohol (PVA, final concentration 0.01 g/L) were added (in ultrapure water) to the H_2O_2 and the process was continued for 45 min. The roles of the additives GA and PVA were to control the size of silver nanoparticles and to confer their steric stability [12,13]. After treatment or cleaning (for the MP specimens), the specimens were placed in a laminar flux hood for drying.

2.2. Surface characterization

Surface morphology, surface composition and cross-sections were investigated by means of scanning electron microscopy (SEM, PHILIPS XL30ESEM) and energy dispersive X-ray spectroscopy (EDS, XMAX Oxford instruments). Cross-sections were prepared by embedding the specimens in epoxy resin that were ground perpendicular to the surface. Ultrasonic cleaning was made in acetone followed by ethanol.

The surface roughness was measured by using a Stylus Profiler (Bruker Dektak XT Precision) and reported as the arithmetic average roughness, Ra, based on analysis of three lines, each 1 mm long, at three different locations of each surface.

Colorimetric measurements were employed to determine changes in surface appearance for the different surfaces using a Minolta CM600D spectrophotometer (D65 light source at 10°) to generate data according to the CIELab color reference space. A digital three-dimensional representation of the color space is described by the L*, a* and b* values where L* represents Lightness, a* the red-green component and b* the blue-yellow component from which a relative change in appearance can be determined and expressed as ΔL*, Δa* and Δb* and whether the change is perceptible or not is determined by $\Delta E^*_{ab} = ((\Delta L^*)^2 + (\Delta a^*)^2 + (\Delta b^*)^2)^{1/2}$. A ΔE^*_{ab} value of 2.3 or higher describes a noticeable change in visual appearance [14]. More details are given in [15].

X-ray photoelectron spectroscopy (XPS) measurements were performed using a Kratos AXIS UltraDLD spectrometer (Kratos Analytical, Manchester, UK) with a monochromatic Al K_α x-ray source (150 W). Instrumental details are given in [10]. Wide spectra and detailed spectra (20 eV pass energy) were collected for Ti 2p, Al 2p, V 2p, Ag 3d, O 1s, C 1s, N 1s and P 2p. All binding energies were corrected to the C 1s peak at 285.0 eV.

2.3. Simulated physiological fluids

All chemicals were of analytical grade (p.a.) or puriss. p.a. (H_2O_2, Sigma Aldrich, Sweden) and ultrapure water was used as solvent (18.2 MΩcm). Bovine serum albumin (BSA, A7906) was purchased from Sigma Aldrich, Sweden. Table 1 shows the composition and pH of the simulated physiological fluids. The selection of solution compositions was based on previous findings [10] and reflects physiologically relevant conditions for benign (PBS) to adverse (PBS + 40 g/L BSA + 30 mM H_2O_2) exposure scenarios.

In the case of the electrochemical measurements, BSA and H_2O_2 were gradually added (every 24 h until the intended solution concentration was reached) during the open circuit potential (OCP) measurements, and in different order to investigate direct effects of BSA and H_2O_2 on the OCP.

2.4. Exposure without applied potential for metal release and particle release studies

Prior to exposure, all vessels and equipment were acid-cleaned in 10 vol.% HNO_3 for at least 24 h, rinsed four times with ultrapure water, and dried in ambient laboratory air. The specimens, with their entire surface areas exposed, were placed in 15 mL polyethylene vessels keeping the surface area to solution volume ratio constant at 1 cm^2/mL. One blank sample (without any specimen), three treated specimens, and three treated-Ag specimens were exposed to PBS + 40 g/L BSA + 10μM H_2O_2, PBS + 30 mM H_2O_2 and PBS + 40 g/L BSA + 30 mM H_2O_2 for 4 h and 2 weeks. For comparison, one MP specimen was exposed in parallel in each solution for 2 weeks. All exposures were conducted at 37 ± 0.5 °C, in dark conditions employing bilinear shaking conditions (12° inclination, 22 cycles/min). This exposure occurred without applied potential, that is, at open-circuit potential.

After exposure, the specimens were removed from the solutions, rinsed with 0.5 mL ultrapure water, dried with nitrogen gas, and stored in a desiccator prior to surface analysis. The test solutions and the rinsing water as this most probably contained precipitated metals and proteins were combined for later metal release analysis. These solutions were centrifuged in an Eppendorf MiniSpin microcentrifuge for 30 min

at 13,400 r.p.m., which corresponds to 12,045 r.c.f., separated into a supernatant and a remaining solution, 0.75 mL and 1 mL, and stored at −20 °C prior to digestion and analysis.

2.5. Electrochemical investigations

All electrochemical measurements were performed using a home-made flat cell with the differently treated surfaces as working electrodes (exposed area 0.502 cm^2), an Ag/AgCl sat. KCl electrode as reference electrode and a platinum mesh as counter electrode in 45 mL PBS (the final volume after complete addition of BSA and H_2O_2). Several flat cells were positioned in a water bath of 37 ± 1 °C. Up to four measurements were run in parallel using a Multichannel Potentiostat (PARSTAT MC).

First, OCP was measured for 1 week either in PBS, in PBS + 40 g/L BSA (added after 24 h), in PBS + 40 g/L BSA (added after 24 h) +30 mM H_2O_2 (added after additional 24 h), or in PBS +30 mM H_2O_2 (added after 24 h) + 40 g/L BSA (added after additional 24 h). For two of these solutions, PBS and PBS + 30 mM H_2O_2 + 40 g/L BSA, additional tests were conducted after the OCP measurement by means of potentiodynamic polarization (PP). The current range was set to 2 µA, since an automatic current range resulted in noisy data for low currents.

After completion of the electrochemical investigations, the specimens were rinsed with 0.5 mL ultrapure water, dried with nitrogen gas and stored in a desiccator prior to surface analysis. The test- and rinsing solutions were stored at −20 °C prior to digestion and solution analysis.

2.6. Digestion and trace metal analysis in solution

Since many of the solution samples contained high amounts of proteins, the solutions were digested prior to trace metal analysis. This process destroys all proteins and any solid silver species in solution [16] and ensures hence accurate quantification. The solution samples that had been incubated without any applied potential (both the supernatant and the remaining solution) were digested for approximately 1 h at 90 °C under ultraviolet irradiation (Metrohm 705 UV digester) by adding 0.5 mL 30 % H_2O_2, 0.15 mL 30 % HCl and ≈8 mL ultrapure water to 0.75 mL of the solution sample until the solution was transparent and odorless. For the solution samples following the electrochemical measurements, unfrozen solutions were diluted by adding 5 mL 65 % nitric acid (HNO_3) and 3 mL ultrapure water to 2 mL of the solution sample followed by digestion using a Milestone Ultraclave for ≈30 min at 180 °C until the solution was transparent and odorless. After the digestion process, the final volumes of all solutions were measured and the dilution factors, DF, were calculated (final volume after digestion divided by the initial solution sample volume).

Released total concentrations of Ti, Al, V, and Ag in the digested solutions were determined by means of graphite furnace atomic absorption spectroscopy (GF-AAS) using a Perkin Elmer AA800 analyst instrument. Calibration standards were based on 1 % HNO_3 and 3–4 standard concentrations up to 45 µg/L (Ag), 80 µg/L (Ti), 100 µg/L (Al) and 120 µg/L (V). Quality control samples of known concentrations were measured every 5th sample to ensure conformity with the calibration. Ultrapure water was analyzed every 2–3 samples to avoid memory effects. Further details are given in [10].

Released and non-precipitated amounts of released metals Me_{aq} (µg/cm^2) were calculated for each solution according to Eq. (1):

$$Me_{aq}\left(\frac{\mu g}{cm^2}\right) = \frac{\left(c_{sample}\left(\frac{\mu g}{L}\right) - c_{blank}\left(\frac{\mu g}{L}\right)\right)*V\,(L)}{A\,(cm^2)}*DF \quad (1)$$

where c_{sample} represents the measured sample concentration, c_{blank} the corresponding blank concentration (amount of metal released into the solution exposed without specimens), V the exposure volume (45 mL), A the exposed surface area of the specimen (cm^2) and DF the dilution factor.

2.7. Photon cross-correlation spectroscopy

Photon cross-correlation spectroscopy (PCCS, NanoPhox, Sympatec GmbH, Germany) dynamic light scattering was used to investigate particle/colloidal size distributions in the supernatant and in remaining solutions after exposure without any applied potential. These solutions were unfrozen a few hours prior to the measurement and were not digested. Two replicate measurements of 120 s were performed on each sample. Initial tests showed that filtering by means of a 0.2 µm membrane (PTFE) lowered the particle/colloidal concentrations to undetectable levels, why most solutions were measured without filtration. Filtration was done on some samples (in which some large particles were present), which were measured before and after filtration. If the correlation function was acceptable (good fitting and no positive values at long lag times), a non-negative least square (NNLS) algorithm was used by the instrument to determine the intensity size distribution. Further details are given in [17].

2.8. Joint expert speciation system modelling

In order to assist in the interpretation of the metal release and corrosion results, chemical speciation modelling was conducted using the Joint Expert Speciation System (JESS, version 8.7, [18]) for Ti, Al, V and Ag in PBS (input: 0.168 M Na^+, 0.15 M Cl^-, 0.0189 M PO_4^{3-}, 0.0099 M K^+, 37 °C, pe 5, pH 7.3), in PBS of higher redox potential (pe 10) to simulate PBS with H_2O_2, and in PBS at varying redox potentials (pe 5 and 10) and presence of amino acids as simulants for BSA. In order to select relevant amino acids, the JESS database was first inspected for available reactions between the metals of interest and different amino acids. In total, 75, 0, 5 and 85 reactions existed in the database for amino acids and Al, Ti, V and Ag, respectively. Since the database included reactions between V and glutamic acid and glycine, but no other amino acids, these acids were used as input settings with molar concentrations (0.0349 M glutamic acid, 0.0102 M glycine) that correspond to their respective concentration in 40 g/L BSA. Since more data was available in the database for Ag and Al, the input settings consist of the predominant amino acids with available reactions, Table 2. Some amino acids were excluded due to absence of reactions (alanine for Al) and errors in the numerical calculations.

2.9. Statistics

A student's *t*-test of unpaired data with unequal variance (KaleidaGraph, version 4.0, Synergy software) was used to test the statistical significance of differences between data sets of independent samples.

Table 2
Input concentrations of amino acids for chemical speciation modelling of Ag and Al in PBS containing 40 g/L BSA at different redox potentials.

Amino acid	Concentration (M) for Al modelling	Concentration (M) for Ag modelling
Alanine	–	0.0289
Arginine	–	0.0157
Aspartic acid	0.0247	
Cysteine	0.0211	
Glutamic acid	0.0349	
Glycine	0.0102	
Histidine	0.00963	
Leucine	0.0391	
Lysine	0.0361	
Serine	0.0193	
Methionine	–	0.00301

Table 3
Arithmetic surface roughness Ra (μm) findings of unexposed and exposed surfaces of mirror-polished, treated and treated-Ag surfaces (mean and standard deviation). Exposure - one week at 37 °C to PBS, PBS + 40 g/L BSA, PBS + 40 g/L BSA + 30 mM H_2O_2 and PBS + 30 mM H_2O_2 + 40 g/L BSA, including potentiodynamic polarization.

Exposure conditions	MP reference	Treated	Treated-Ag
Unexposed	0.05 ± 0.01	0.24 ± 0.01	0.26 ± 0.04
PBS	N/A	0.23 ± 0.01	0.29 ± 0.04
PBS + BSA	N/A	0.25 ± 0.01	0.31 ± 0.04
PBS + BSA + H_2O_2	N/A	0.29 ± 0.01	0.29 ± 0.02
PBS + H_2O_2 + BSA	0.055 ± 0.008	0.29 ± 0.01	0.29 ± 0.04

N/A – not analyzed.

3. Results and discussion

3.1. Porosity, surface roughness, oxide thickness, and visual appearance

The chemical surface treatments of Ti6Al4V resulted in considerably different visual appearances ($\Delta E > > 2.3$) compared with the MP surfaces. The treated surfaces gained a reddish-bluish surface appearance ($\Delta E = 25$ *vs.* MP) and the treated-Ag surfaces a yellowish appearance ($16 < \Delta E < 30$ *vs.* MP), see Fig. S1 (supplementary information). The MP surfaces did not show any significant change in appearance ($\Delta E < 2.3$) after exposure in PBS, but small though significant ($3 < \Delta E < 7$) differences after exposure into the more complex physiological environments. Pronounced differences in appearance after exposure were also evident for the treated surfaces compared with their corresponding unexposed surfaces, even though large variations were observed between surfaces of different batches ($8 < \Delta E < 18$). No measurements were made on the exposed treated-Ag surfaces due to large variations in surface appearance for the unexposed surfaces.

The surfaces of the treated and treated-Ag Ti6Al4V alloy were significantly ($p < 0.001$) rougher compared to the MP reference, Table 3, whereas the difference between the treated and treated-Ag surfaces was small. SEM investigations of cross-sections revealed a slightly thicker surface oxide for the exposed treated and treated-Ag specimens as compared to the exposed MP reference, Fig. S2 (supplementary information). Exposure to PBS + 40 g/L BSA + 30 mM H_2O_2 resulted in a slightly thicker surface oxide as compared with exposure to PBS.

From the SEM investigation it is evident that the surface roughness of the treated surfaces derives from a porous structure with pores sized ≈1 μm, Fig. 1, as well as nano-sized features within the pores, as illustrated in the insets of Fig. 1d–e. Ag was non-homogenously distributed on the surface of the treated-Ag alloy showing μm-sized aggregates of Ag nanoparticles (confirmed by EDS spot analysis), Fig. 1. Based on the SEM investigation, no consistent results were possible to obtain on their stability in the exposed solutions as some exposed surfaces showed the absence of these Ag aggregates and others their presence, Fig. S3 (supplementary information).

3.2. OCP changes as a function of solution and time

Fig. 2 shows representative OCP curves of the MP and treated-Ag surfaces exposed to the different solutions. The MP reference (non-freshly polished) revealed an initial OCP of between −300 and −100 mV (vs. Ag/AgCl sat. KCl) in PBS (37 °C), Fig. 2. These potentials are in accordance with previous findings for Ti6Al4V alloys at similar conditions [6–8]. An initially more positive OCP (50 − 200 mV) was observed for the treated-Ag surfaces, most probably due to their thicker oxide, Fig. 2. The OCP increased with time in PBS for all surfaces of Ti6Al4V during the first day of exposure. The H_2O_2 addition after one or two days of exposure substantially increased the OCP for all surfaces. In contrast, the BSA addition into PBS decreased the OCP when added after one day. However, this decrease was negligible after two days of exposure in both PBS and PBS with the previous addition of H_2O_2, Fig. 2. An increased OCP due to the addition of H_2O_2 and a decreased OCP connected to the addition of BSA are consistent with previous findings [7,8,10]. The increased OCP has been explained by the oxidative action of H_2O_2 [19,20], and the initially decreased OCP by the adsorption of BSA has been linked to its blocking of cathodic sites [7,8,10,21]. This does however not mean that BSA inhibits corrosion or metal release after longer time periods [7,9].

3.3. Corrosion investigations by means of potentiodynamic polarization

Fig. 3 shows representative curves of changes in current density with applied potential after one week of preceding exposure to PBS (Fig. 3a) and PBS + 30 mM H_2O_2 + 40 g/L BSA (Fig. 3b). The corrosion potential was, like the OCP shown in Fig. 2, for the same reasons more positive in PBS containing H_2O_2 and for the treated surfaces compared to the MP reference. This increase was statistically significant in all cases except one (treated-Ag in PBS + 30 mM H_2O_2 + 40 g/L BSA compared with PBS), see Table S2, supplementary information. It is clear from Figs. 3 and S4 (supplementary information) that the passive range was for all specimens smaller in the more corrosive solution PBS + 30 mM H_2O_2 + 40 g/L BSA compared with PBS. Further, there were a statistically lower corrosion potential and OCP value for the treated-Ag specimen compared to the treated specimen in the most corrosive solution PBS + 30 mM H_2O_2 + 40 g/L BSA. The passive current density was to a relatively small extent affected by the treatment and synthetic solution for the treated and non-treated surfaces without Ag. The treated-Ag surfaces showed slightly higher passive current densities (440 − 680 nA/cm^2) in the most corrosive solution (Table S1) compared to PBS (150 nA/cm^2) and compared with observations for the other surfaces (83 − 400 nA/cm^2), however, this difference was not statistically significant. Despite the substantially larger surface area due to the porous structure of the treated specimens, their passive current densities were not significantly larger as compared to the MP specimen. Previous studies of Ti6Al4V coupled with and without Ag report a corrosion current density of 9 nA/cm^2 for the non-coupled alloy, and current density of 24 nA/cm^2 for the coupled alloy after 10 days in 0.9 % NaCl [6]. It seems that the porous TiO_2-rich surface treatment to some extent can hinder galvanic effects induced by the Ag coupling in PBS. Whether this protective effect of the surface treatment is also functional under more corrosive conditions, such as in PBS + 30 mM H_2O_2 + 40 g/L BSA, needs to be investigated in future studies.

3.4. Metal release of metal species and particles without applied potential

The relative composition of metals (oxidized and metallic) in the outermost surface (top 5 − 10 nm) measured by means of XPS is shown in Fig. 4. A significantly higher fraction of carbon (C2: 286.3 ± 0.2 eV related to peptidic residues, C−O and C−N bonds, and C3: 288.2 ± 0.1 eV related to N−C=O bonds [22]) and nitrogen (400.1 ± 0.1 eV) was observed for surfaces exposed to PBS containing 40 g/L BSA compared with corresponding unexposed surfaces and surfaces exposed to PBS + 30 mM H_2O_2 ($p < 0.0001$). The observed atomic ratio of N/(C2 + C3), which theoretically equals to 0.48 for BSA [23], was 0.41 ± 0.11 on surfaces exposed to BSA and significantly ($p < 0.0001$) higher compared to corresponding exposures without BSA (0.20 ± 0.08). This indicates the presence of adsorbed BSA that was not possible to remove by the rinsing procedure. Ag ($3d_{5/2}$: 368.1 ± 0.2 eV) was only detected in its metallic form and only for the treated-Ag surfaces, Fig. 4. Seemingly lower and varying concentrations of Ag for the exposed surfaces (c.f. Fig. 1) compared with the non-exposed surfaces were related to its heterogeneous surface distribution. Except for the MP surfaces exposed for 4 h in PBS + 10 μM H_2O_2 + 40 g/L BSA, for which Ti was observed in its metallic state ($2p_{3/2}$: 454.1 ± 0.9 eV), Fig. 4, all other surfaces revealed Ti in its oxidized state ($2p_{3/2}$: 458.6 ± 0.3 eV) related to Ti(IV) [24]. When observed

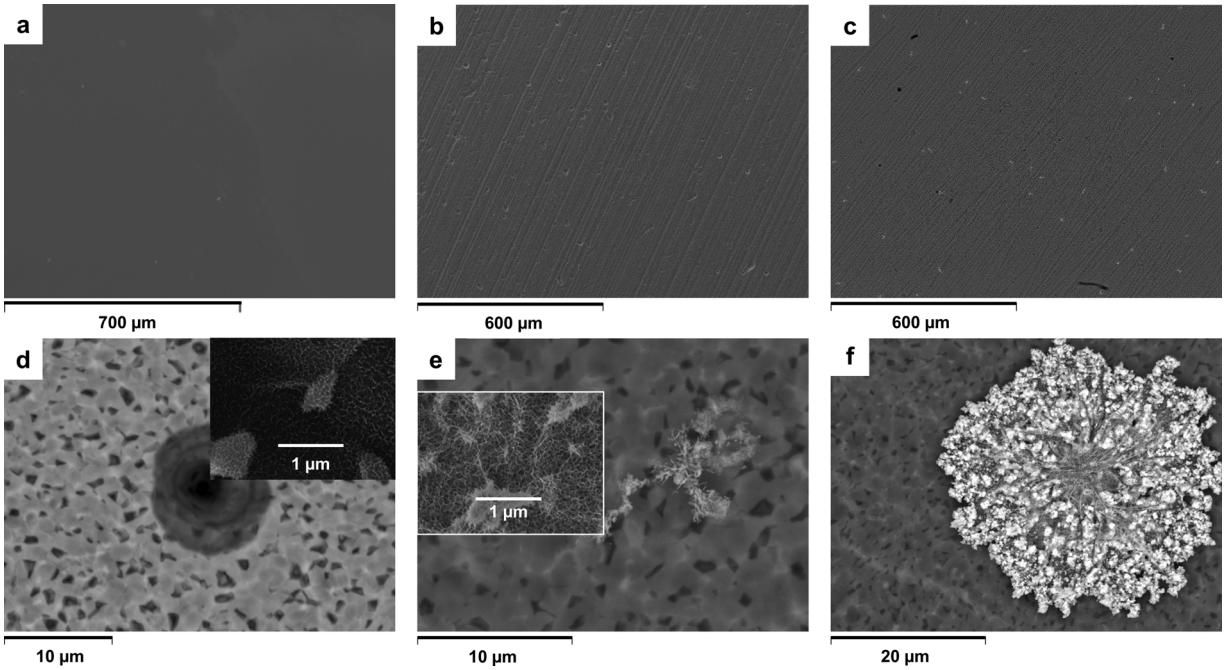

Fig. 1. SEM backscatter images of the MP reference (a), the treated- (b, d) and the treated-Ag surfaces of Ti6Al4V (c, e, f) at different magnifications. Insets in (d, e) at higher magnification.

(for both unexposed and exposed surfaces), Al was present in its oxidized form as Al(III) [25] (2p: 74.6 ± 0.3 eV). V was only detected on the unexposed non-treated MP surface and was present as V(IV) [24] ($2p_{3/2}$: 516.4 ± 0.3 eV). In agreement with previous findings [10], the relative composition of oxidized metals within the outermost surface oxide (top 5 − 10 nm) of the unexposed MP reference surface was 88.4 wt% Ti, 7.1 wt% Al and 4.5 wt% V, i.e. not very different from the bulk composition of Ti6Al4V. Oxidized V was not detected in any of the exposed (or unexposed treated) surfaces, an observation that was considered to be related to its high solubility in given solutions as in agreement with previous observations [10]. An evident difference was observed in the relative Al content of the outermost surface oxide for the Ti6Al4V surfaces exposed to non-protein conditions compared with solutions containing BSA, Fig. 4. No or considerably lower relative contents of oxidized Al in the surface oxides were observed for any Ti6Al4V surface or exposure time period when exposed in PBS containing 40 g/L BSA compared to exposures in PBS + 30 mM H_2O_2 without any BSA, Fig. 4. In the protein-free solution, the relative Al content clearly increased after 2 weeks of exposure compared to the unexposed both non-treated and treated Ti6Al4V surfaces. This observation supports our previous hypothesis [10] that Al becomes enriched in the surface oxide of Ti6Al4V upon exposure in PBS in the presence of H_2O_2 and absence of BSA due to the formation of a slightly soluble TiOOH-complex [26,27], but depleted in the presence of BSA due to complexation-induced Al dissolution of the surface oxide [28]. This effect (bonding of BSA to Al in the surface oxide) has previously been suggested to be of relatively higher importance in the presence of H_2O_2 due to the formation of a more defect-rich surface oxide [10].

Total amounts of released Ti, Al, V and Ag from the MP, treated and treated-Ag surfaces of Ti6Al4V were analyzed after 4 h and 2 weeks of incubation in PBS at 37 °C with BSA (40 g/L) and varying H_2O_2 content (10 µM or 30 mM), and in PBS with H_2O_2 (30 mM) without BSA. Since there were small differences in metal concentrations in the centrifuged supernatant and the remaining solutions, the total amount of released metals was normalized to the geometric surface area, see Fig. 5. In accordance with the XPS investigations, Ti was the predominant metal

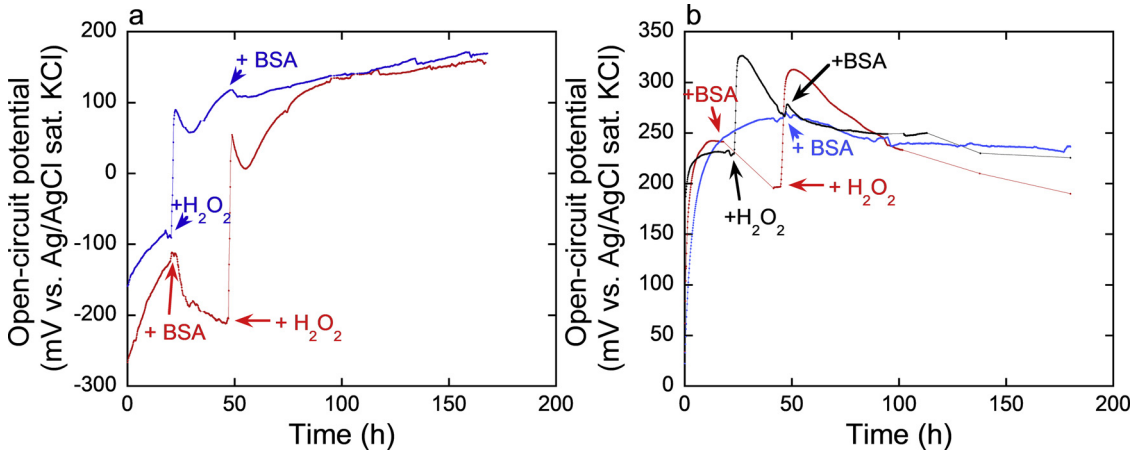

Fig. 2. Representative OCP curves with time (up to one week) for MP (a) and treated-Ag Ti6Al4V (b) exposed in PBS at 37 °C for one day, followed by the addition of 40 g/L BSA or 30 mM H_2O_2 (as indicated in the same color of the curve) after one and/or two days.

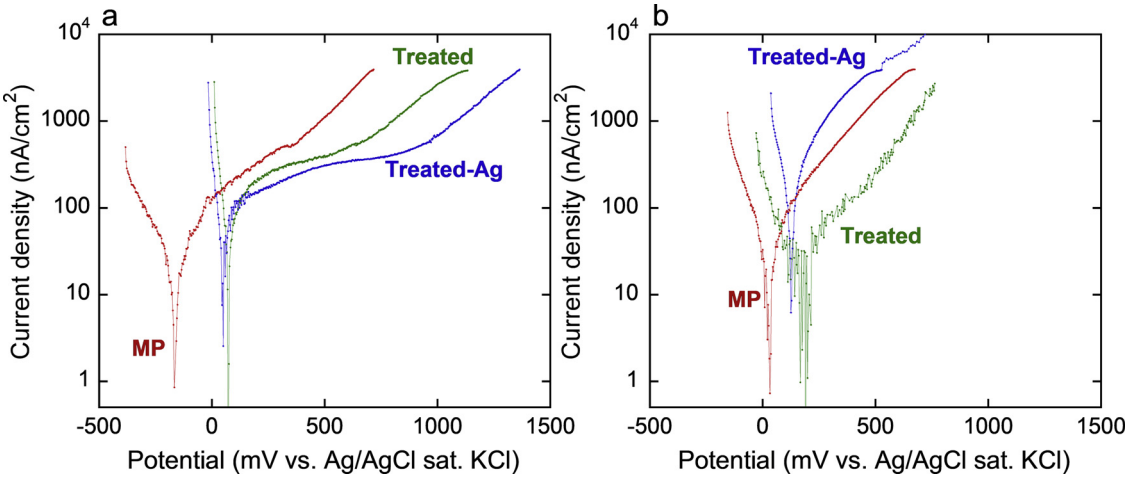

Fig. 3. Representative current density – potential curves for the MP reference, the treated and treated-Ag surfaces of Ti6Al4V in PBS (a) and in PBS +30 mM H_2O_2 + 40 g/L BSA (b) after one week of exposure at 37 °C. For information on variability between replicate measurements, see Fig. S4, supplementary information.

released from the non-treated (MP) and both treated surfaces. Both Ti and Ag were predominantly released from the treated-Ag specimen. The metal release process was both time- and solution dependent, Fig. 5. In accordance with the XPS interpretation of Al depletion from the surface oxide in BSA-rich solutions, substantially more Al was released for all surfaces after 2 weeks of exposure in PBS +30 mM H_2O_2 + 40 g/L BSA compared to their performance in PBS +30 mM H_2O_2. V was released to a higher extent from the MP surface compared to the treated and treated-Ag surfaces, Fig. 5. This is most probably related to a depletion of V from the surface during the surface modification treatment, as indicated by the absence of V in the surface oxide of unexposed treated and treated-Ag specimens (Fig. 4). Ag was only released from the treated-Ag specimen and to a considerably higher extent in the presence of BSA. This suggests a complexation-induced dissolution mechanism, further discussed Section 3.5. It should be noted that the released amounts of metals presented in Fig. 5 are normalized to the geometric surface area and not to the effective surface area (which increases with increased surface roughness). Considering the large difference in surface roughness and presence of pores between the MP reference and the two treated surfaces (c.f. Section 3.1.), it is evident that the increased surface area induced by the treatment to gain an enhanced bone bonding ability did not result in an increased extent of released metals under the given conditions of this study. This is most probably related to a passivation effect of the treatment.

Dynamic light scattering using PCCS revealed no detectable particles/colloids for solutions without BSA (such as PBS), whereas solutions containing BSA contained colloids sized between 7.6 and 13 nm, indicative of BSA [17,29]. This was observed both for blank solutions (no Ti6Al4V surfaces) and for solutions with exposure to the Ti6Al4V specimens. No significant trend was observed regarding the average colloidal size for the supernatants (centrifuged) and non-supernatant solutions, or for the solutions containing varying amounts of H_2O_2 (PBS + 10 μM H_2O_2 + 40 g/L BSA and PBS +30 mM H_2O_2 + 40 g/L BSA) after 4 h and 2 weeks of exposure to the different surfaces. Higher count rates (96 ± 21 kcounts/s after 2 weeks) were observed for solutions that had been in contact with the treated-Ag surfaces compared with blank solutions (no treated-Ag surfaces) or solutions from exposures with the treated surfaces after the same time periods (49 ± 33

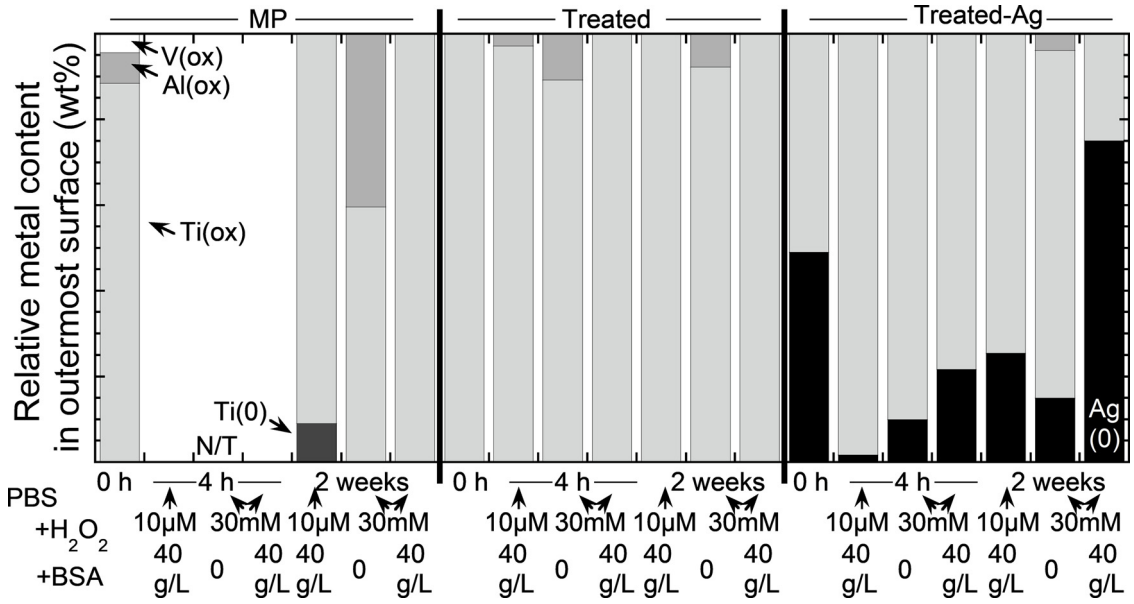

Fig. 4. Relative (wt%) metal composition of Ti, Al, V and Ag in the outermost surface (5-10 nm) of unexposed (0 h) or exposed surfaces of Ti6Al4V (MP, treated and treated-Ag). The data reflects mean values (n = 4) of duplicate measurements (two separate areas sized ≈0.4 mm^2 on each surface) for two independent specimens of each surface (one specimen for MP). N/T – not analyzed/tested; ox - oxidized. Ti(0) and Ag(0) denote their metallic states.

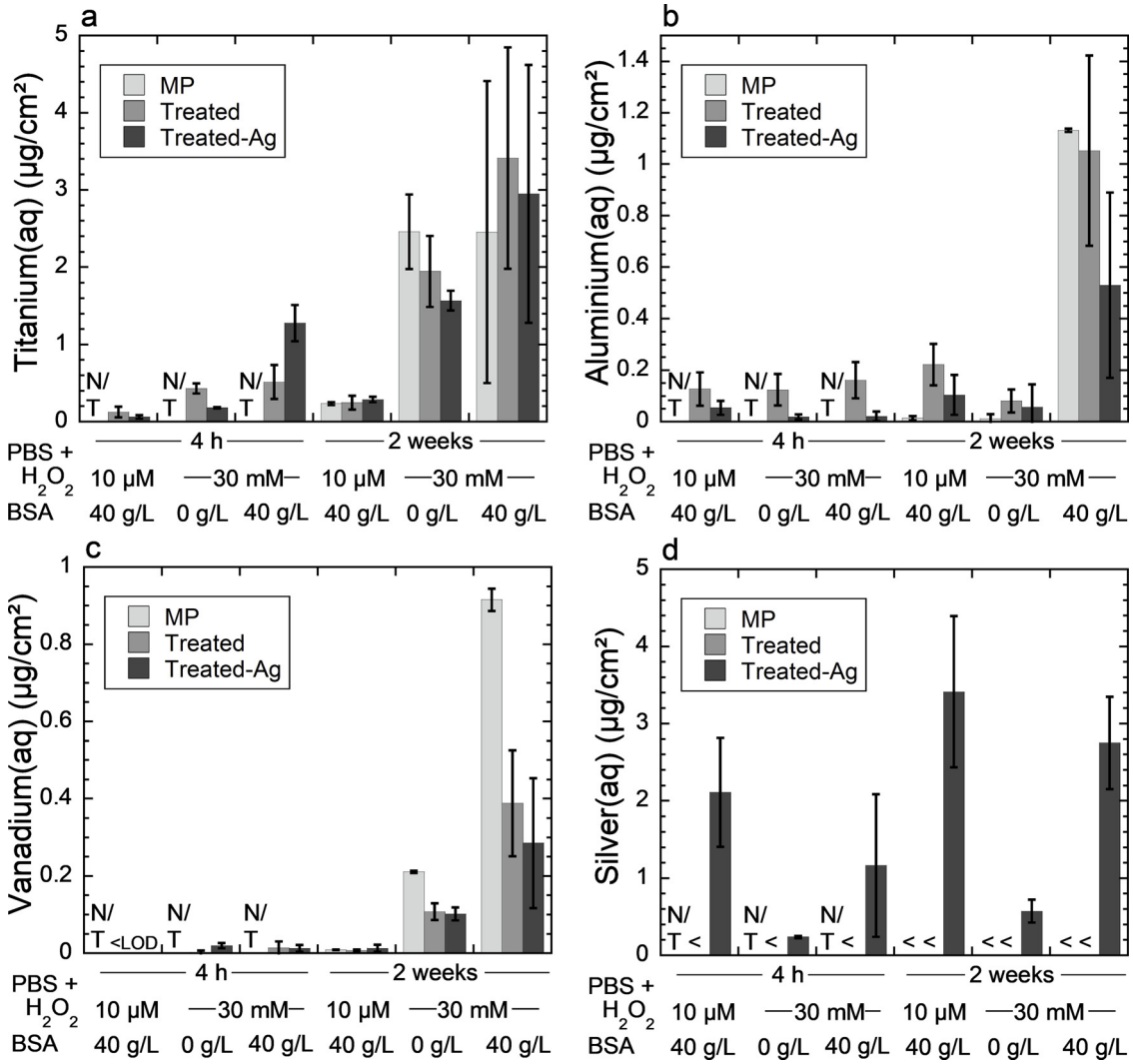

Fig. 5. Released and non-precipitated amounts of Ti (a), Al (b), V (c) and Ag (d) from MP, treated and treated-Ag surfaces of Ti6Al4V incubated for 4 h and 2 weeks in PBS (pH 7.3, 37 °C) containing varying amounts of H_2O_2 and BSA without applied potential (at OCP). The error bars show the standard deviation of triplicate surfaces (treated, treated-Ag), and of six solution sample readings for one specimen (MP). Blank (background) concentrations are subtracted. Note the different y-axis scales.

kcounts/s) ($p < 0.0005$). This indicates the possible presence of some Ag colloidal particles and/or protein agglomeration (caused by released Ag ions/nanoparticles from the treated-Ag surfaces).

3.5. Metal release after polarization and chemical speciation modelling

The chemical speciation modelling, Table 4, predicted Ti to be sparingly soluble (16 % of 10 µM) in PBS with and without H_2O_2, Table 4. No predictions of the speciation of Ti in the presence of BSA

Table 4
Predominant species in solution of released metals and solution ligands according to chemical speciation modelling for a concentration of 10 µM metal (Ti, Al, V or Ag) in PBS (37 °C, pH 7.3) with and without H_2O_2 and BSA (simulated by amino acids). s – solid; aq – aqueous. N/R – no reactions available in the database.

Input values simulating	Ti	Al	V	Ag
PBS	84% TiO_2 (s), 16% $TiOCl_4^{2-}$ (aq)	δ-Al_2O_3 (s)	H_3VO_4 (s)	72% $AgCl_2^-$ (aq), 19% $AgCl_3^{2-}$ (aq), 7% AgCl (aq), 1% $AgCl_4^{3-}$ (aq), 1% Ag (aq)
PBS + 30 mM H_2O_2				73% $AgCl_2^-$ (aq), 19% $AgCl_3^{2-}$ (aq), 7% AgCl (aq), 1% $AgCl_4^{3-}$(aq)
PBS + 40 g/L BSA PBS + 30 mM H_2O_2 + 40 g/L BSA	N/R	$AlC_6H_{10}N_2O_4S_2^-$ (aq)	89% H_3VO_4 (s), 11% $VO_2H_2NCH_2CO_2^-$ (aq)	$AgC_3H_5NO_2S^-$(aq)

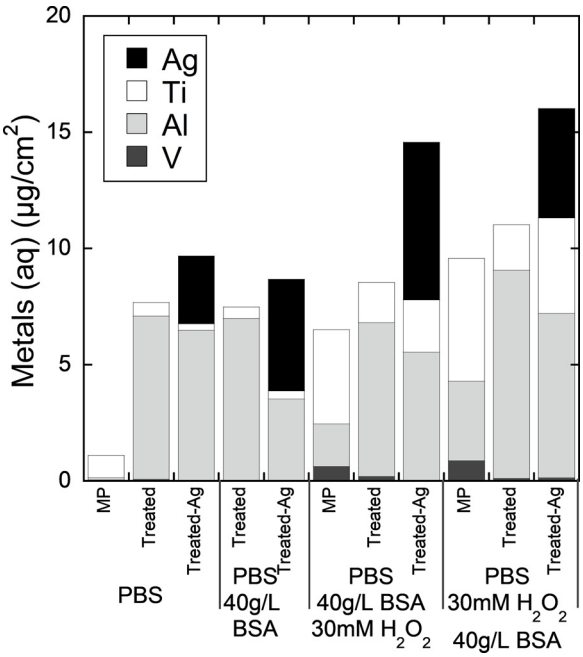

Fig. 6. Non-precipitated amounts of Ti, Al, V, and Ag released from the MP surface (one specimen), treated (two specimens) and treated-Ag surfaces (three specimens) in PBS solutions (37 °C) of different BSA and H_2O_2 concentrations (added in sequence, c.f. Fig. 2 and Table 1) after one week at OCP and subsequent potentiodynamic polarization to +1 V vs. OCP. Blank concentrations are subtracted.

were possible due to the lack of reactions between Ti and amino acids in the database. Al was predicted insoluble in solutions without BSA, but soluble in solutions containing amino acids (at concentrations corresponding to 40 g/L BSA) related to the formation of a cysteine complex. V was predicted sparingly soluble only in solutions with BSA (11 % of 10 µM), forming a complex with glycine. Ag was foreseen to be soluble in all solutions forming complexes with chlorides in solutions without BSA and complexes with cysteine in solutions with BSA.

Solution concentrations of all released metals in solution were in addition determined after potentiodynamic polarization (after one-week preceding OCP conditions) of the Ti6Al4V surfaces, Fig. 6. The polarization step is expected to result in drastically increased metal ion concentrations in solution compared to OCP conditions (Fig. 5). However, this was not the case for either Ti or V that showed comparable results with findings at OCP conditions (c.f. Figs. 5 and 6). This suggests that their released concentrations were governed by solubility constraints (precipitation) and therefore most probably underestimated (at least for the polarized surfaces). Released amounts of Ti after polarization were consistently lower for all treated and treated-Ag surfaces and solutions compared to the MP reference surface, findings which further indicate a passivation effect of the surface modification treatment. Similar to findings for released Ti and V, comparable (only slightly higher) concentrations of released Ag were observed from the polarized surfaces compared to findings at OCP-conditions. Slightly more Ag was further released under conditions including BSA ($p = 0.05$), which suggests that bonding between Ag and BSA plays a role for the metal release process. Enhanced release of Ag from Ag metal surfaces due to surface complexation and enhanced exchange rates of surface complexes with BSA molecules in solution have previously been reported [30]. In this study, the extent of Ag release was though limited by the low amount of surface-accessible Ag nanoparticles/aggregates, see Fig. 1. Released amounts of Al were negligible for the polarized reference surfaces (MP) in PBS, but considerably higher for the differently treated surfaces in all solutions and MP in other solutions compared to their corresponding behavior at OCP-conditions. The release of Al was further higher for the treated and treated-Ag surfaces compared to the MP reference at all conditions ($p < 0.01$). In all, the results suggest that polarization enhances the combined BSA- and H_2O_2-induced Al release process, and that the surface modification treatment made to gain an enhanced bone bonding ability results in increased levels of Al release upon oxidation (anodic polarization). The latter is unexpected in PBS without BSA (Table 4) from a chemical speciation modelling perspective and may probably be related to kinetic effects (slow formation and precipitation of Al_2O_3).

3.6. Further discussion

Findings of this study support an earlier proposed mechanism of the combined action of H_2O_2 and BSA on metal release and corrosion of Ti6Al4V alloys [7,8,10]. It further shows the mechanism to be valid also for relatively thick and more passive surface oxides (in this case optimized to gain an enhanced bone bonding ability) compared to the native oxide of a non-treated alloy. Even though these thick surface oxides predominantly were composed of oxidized titanium (Ti(IV) – TiO_2), the enrichment of Al in the outermost surface was observed when exposed to H_2O_2-rich conditions, and a depletion of Al occurred under conditions containing BSA. Only when both BSA and H_2O_2 were present at concentrations of relevance for inflammatory conditions and infections [10,31], considerably enhanced effects were observed from both a corrosion and metal release perspective. It has recently been discussed [9,10,32,33] that the test conditions of the most corrosive solution of this study could be used to realistically simulate severe human body conditions of biomedical alloys since obtained results both resemble the metal release pattern observed in-vivo [34,35] and in other corrosive simulated physiological fluids such as PBS with 1% lactic acid, 1.2 % L-Cysteine, and 0.01 % HCl after one week of exposure [36].

As suggested earlier [10], the results of this study show an evident risk of underestimating the extent of released Ti (and in some cases also of Al and V) under given or similar test conditions due to precipitation effects of released metals. Such effects were in this study both elucidated by the results of the chemical speciation modelling and seemingly underestimated levels of released amount of Ti determined in solution after potentiodynamic polarization.

It should be noted that measured amounts of released Ti, Al and V in this study were relatively low and that all exposures were performed at passive and aged conditions (1–3 months since the reference surfaces of MP were polished at the same occasion as the treated specimens were prepared). Observed amounts of released metals from the MP specimen were hence lower than reported in a recent study [10] performed under similar conditions on more freshly polished (one day aged) surfaces. The results indicate improved passive properties of the native oxide with time in air.

Compared with the release of Ti, Al and V, the release of Ag was strongly dependent on the presence of BSA and less dependent on the presence of H_2O_2. The chemical speciation modelling suggested BSA-induced Ag release due to bonding of Ag to cysteine-rich binding sites of BSA. Enhanced dissolution of Ag from Ag metal has previously been reported in the presence of BSA proposing a surface complexation mechanism [30]. Silver nanoparticles have also previously been reported to spontaneously bind to BSA at a single binding site [37]. In this study, the PCCS results indicate larger colloids in solutions containing BSA in contact with the treated-Ag specimen compared to BSA solutions in contact with the treated (no Ag) and blank (no specimens) solutions. These colloids could either be Ag nanoparticles and/or protein aggregates induced by binding to silver nanoparticles or ions. The Ag^+ ion has been reported to bind strongly at one binding site to BSA and weakly (at high Ag^+ concentrations) to an additional site primarily via van der Waals interactions at low Ag^+ to BSA ratios and via electrostatic interactions for high ratios [38]. It was in this study not possible to determine whether released Ag was present as ions or as nanoparticles in solution, however, the BSA-induced increase of Ag release

indicates at least some bonding to BSA. The release of Ag was in this study initially relatively rapid and increased after 4 h only slightly up to 2 weeks of exposure.

Galvanic effects of the coupled system Ag – Ti6Al4V might theoretically cause an increased extent of corrosion and metal release. Such effects have been reported for a potentiodynamically polarized Ag/Ti6Al4V system in 0.9 % saline [6], though Ag was coated on the Ti6Al4V surface without any oxide thickening procedure (commonly used to optimize the bone bonding ability). The thick surface oxide of the treated-Ag surfaces in this study might explain why galvanic effects induced by Ag were minor. Some indications were observed that galvanic effects took place in the most corrosive solution, but this could not be concluded with certainty and requires further studies. No increased extents of released Ti, Al or V were observed at OCP of the treated-Ag surfaces compared with the Ag-free treated surfaces. Observed passive current density values of this study were higher compared to the study on Ag-coated Ti6Al4V in 0.9 % saline [6]. This is most probably related to a larger (porous) effective surface area and more corrosive solutions. The results indicate that galvanic effects could play a role at corrosive conditions, aspects that need further studies and should be considered in the development and optimization of antimicrobial biomedical Ti6Al4V alloys.

One of the strengths of this study is that it investigated relevant implant materials in relevant simulated physiological environments. However, the heterogeneity of Ag nanoparticles on the treated-Ag specimens, the high protein concentrations, the concomitant chemical and electrochemical reactions, and the solution composition resulting in precipitation of some metal species may result in larger data variability and less mechanistically detailed conclusions than would be possible for a more simplified system.

4. Conclusions

The aims of this investigation were to study possible galvanic effects induced by the presence of Ag and effects of BSA and H_2O_2 on chemically treated Ti6Al4V surfaces (modified to gain an enhanced bone bonding ability, with and without antimicrobial Ag) in simulated physiological solutions from a combined metal release and corrosion perspective. The following main conclusions were drawn:

1 Despite the larger surface area of the chemically treated surfaces of higher surface roughness and the presence of pores compared to the non-treated reference surface (MP), measured passive current densities and amounts of released metals were similar.
2 For all surfaces of the Ti6Al4V alloy, increased levels of metal release and corrosion were observed in the presence of both H_2O_2 and BSA. H_2O_2 caused Al to be enriched in the outermost surface oxide, and BSA depleted Al due to Al-BSA complexation reactions at the surface and in solution.
3 Released amounts of Ag were enhanced in all solutions containing BSA compared to BSA-free solutions.
4 The chemical speciation modelling results and the metal release findings after potentiodynamic polarization of the non-treated and treated surfaces highlight that precipitation of released Ti, Al and V species take place in solutions without BSA and of released Ti in solutions with BSA. These limitations in solubility make the system sensitive to experimental settings such as surface area to solution volume ratio and sampling time periods, which are aspects that need to be considered when designing simulated physiological test conditions for alloys such as Ti6Al4V.
5 The electrochemical measurements gave some indications on a larger decrease in corrosion resistance for the treated-Ag surface as compared to the Ag-free treated and non-treated specimens in the most corrosive solution (PBS +30 mM H_2O_2 + 40 g/L BSA, 37 °C), although the differences were small or non-significant. The Ag-treated alloy showed a lower corrosion potential as compared to the treated alloy in the most corrosive solution after one week of exposure. Further studies are required to assess any galvanic effects of Ag nanoparticles for the titanium alloy in corrosive environments of relevance for inflammatory conditions.

Funding

Swedish Research Council (VR, grant no. 2015–04177), faculty resources at KTH, and MAECI (Ministero degli Affari Esteri e Cooperazione Internazionale-Italia) are acknowledged for funding (GLOBAL progetti di grande rilevanza internazionale).

Data availability statement

Raw data are available on the platform Open Science Framework (https://osf.io/s346n/).

CRediT authorship contribution statement

Yolanda S. Hedberg: Conceptualization, Methodology, Validation, Formal analysis, Writing - original draft, Visualization, Supervision, Project administration, Funding acquisition. **Francesca Gamna:** Methodology, Validation, Formal analysis, Investigation. **Gianmaria Padoan:** Investigation. **Sara Ferraris:** Supervision. **Martina Cazzola:** Supervision. **Gunilla Herting:** Methodology, Supervision. **Masoud Atapour:** Formal analysis, Writing - review & editing. **Silvia Spriano:** Conceptualization, Resources, Writing - review & editing, Supervision, Funding acquisition. **Inger Odnevall Wallinder:** Conceptualization, Investigation, Writing - review & editing.

Declaration of Competing Interest

None.

Acknowledgements

Dr. Jonas Hedberg and Zheng Wei, both at KTH, are highly acknowledged for assistance in supervision and measurements. Dr. Cem Örnek is acknowledged for valuable discussions.

Appendix A. Supplementary data

Supplementary material related to this article can be found, in the online version, at doi:https://doi.org/10.1016/j.corsci.2020.108566.

References

[1] S. Spriano, S. Yamaguchi, F. Baino, S. Ferraris, A critical review of multifunctional titanium surfaces: new frontiers for improving osseointegration and host response, avoiding bacteria contamination, Acta Biomater. 79 (2018) 1–22.
[2] M. Navarro, A. Michiardi, O. Castaño, J.A. Planell, Biomaterials in orthopaedics, J. R. Soc. Interface 5 (2008) 1137–1158.
[3] S. Spriano, S. Ferraris, G. Pan, C. Cassinelli, E. Vernè, Multifunctional titanium: surface modification process and biological response, J. Mech. Med. Biol. 15 (2015) 1540001.
[4] S. Ferraris, A. Cochis, M. Cazzola, M. Tortello, A. Scalia, S. Spriano, L. Rimondini, Cytocompatible and anti-bacterial adhesion nanotextured titanium oxide layer on titanium surfaces for dental and orthopaedic implants, Front. Bioeng. Biotechnol. 7 (2019) 103.
[5] S. Ferraris, A. Venturello, M. Miola, A. Cochis, L. Rimondini, S. Spriano, Antibacterial and bioactive nanostructured titanium surfaces for bone integration, Appl. Surf. Sci. 311 (2014) 279–291.
[6] M. Furko, M. Lakatos-Varsányi, C. Balázsi, Complex electrochemical studies on silver-coated metallic implants for orthopaedic application, J. Solid State Electrochem. 20 (2016) 263–271.
[7] Y. Zhang, O. Addison, F. Yu, B.C.R. Troconis, J.R. Scully, A.J. Davenport, Time-dependent enhanced corrosion of Ti6Al4V in the presence of H2O2 and albumin, Sci. Rep.-UK 8 (2018) 3185.
[8] F. Yu, O. Addison, A.J. Davenport, A synergistic effect of albumin and H2O2 accelerates corrosion of Ti6Al4V, Acta Biomater. 26 (2015) 355–365.
[9] Y.S. Hedberg, Role of proteins in the degradation of relatively inert alloys in the

human body, Npj Mater. Degrad. 2 (2018) 26.
[10] Y.S. Hedberg, M. Žnidaršič, G. Herting, I. Milošev, I. Odnevall Wallinder, Mechanistic insight on the combined effect of albumin and hydrogen peroxide on surface oxide composition and extent of metal release from Ti6Al4V, J. Biomed. Mater. Res. Part B Appl. Biomater. 107 (2019) 858–867.
[11] S. Spriano, E. Vernè, S. Ferraris, Multifunctional titanium surfaces for bone integration, European Patent, 2214732 (2010).
[12] S. Ferraris, S. Spriano, M. Miola, E. Bertone, V. Allizond, A. Cuffini, G. Banche, Surface modification of titanium surfaces through a modified oxide layer and embedded silver nanoparticles: effect of reducing/stabilizing agents on precipitation and properties of the nanoparticles, Surf. Coat. Tech. 344 (2018) 177–189.
[13] S. Spriano, E. Vernè, S. Ferraris, Process for producing multifunctional titanium surfaces for reducing the risk of infection and increased bone integration and product made through process, in, PCT patent pending no. PCT-IT2012-000237, 2012.
[14] G. Sharma, Digital Color Imaging Handbook, CRC Press, Boca Raton, FL, USA, 2003.
[15] Consiglio Nazionale delle Ricerche, Normal - 43/93: Misure colorimetriche strumentali di superfici opache, CNR-ICR, Rome, 1994.
[16] J. Hedberg, S. Skoglund, M.-E. Karlsson, S. Wold, I. Odnevall Wallinder, Y.S. Hedberg, Sequential studies of silver released from silver nanoparticles in aqueous media simulating sweat, laundry detergent solutions and surface water, Env. Sci. Technol. 48 (2014) 7314–7322.
[17] Y.S. Hedberg, I. Dobryden, H. Chaudhary, Z. Wei, P. Claesson, C. Lendel, Synergistic effects of metal-induced aggregation of human serum albumin, Colloids Surf. B Biointerfaces 173 (2019) 751–758.
[18] P.M. May, D. Rowland, Thermodynamic modeling of aqueous electrolyte systems: current status, J. Chem. Eng. Data 62 (2017) 2481–2495.
[19] J.L. Wang, R.L. Liu, T. Majumdar, S.A. Mantri, V.A. Ravi, R. Banerjee, N. Birbilis, A closer look at the in vitro electrochemical characterisation of titanium alloys for biomedical applications using in-situ methods, Acta Biomater. 54 (2017) 469–478.
[20] J. Pan, D. Thierry, C. Leygraf, Hydrogen peroxide toward enhanced oxide growth on titanium in PBS solution: blue coloration and clinical relevance, J. Biomed. Mater. Res. 30 (1996) 393–402.
[21] L. Dragus, L. Benea, N. Simionescu, A. Ravoiu, V. Neaga, Effect of the inflammatory conditions and albumin presence on the corrosion behavior of grade 5 titanium alloy in saliva biological solution, IOP Conference Series: Materials Science and Engineering, IOP Publishing, 2019, p. 012005.
[22] B. Wu, C. Mu, G. Zhang, W. Lin, Effects of Cr3+ on the structure of collagen fiber, Langmuir 25 (2009) 11905–11910.
[23] K. Hirayama, S. Akashi, M. Furuya, K.-I. Fukuhara, Rapid confirmation and revision of the primary structure of bovine serum albumin by ESIMS and frit-FAB LC/MS, Biochem. Biophys. Res. Commun. 173 (1990) 639–646.
[24] M.C. Biesinger, L.W. Lau, A.R. Gerson, R.S.C. Smart, Resolving surface chemical states in XPS analysis of first row transition metals, oxides and hydroxides: Sc, Ti, V, Cu and Zn, Appl. Surf. Sci. 257 (2010) 887–898.
[25] J.A. Rotole, P.M. Sherwood, Gamma-alumina (γ-Al2O3) by XPS, Surf. Sci. Spectra 5 (1998) 18–24.
[26] P. Tengvall, H. Elwing, I. Lundström, Titanium gel made from metallic titanium and hydrogen peroxide, J. Colloid Interf. Sci. 130 (1989) 405–413.
[27] P. Tengvall, I. Lundström, L. Sjöqvist, H. Elwing, L.M. Bjursten, Titanium-hydrogen peroxide interaction: model studies of the influence of the inflammatory response on titanium implants, Biomaterials 10 (1989) 166–175.
[28] S. Fatemi, F.H. Kadir, G.R. Moore, Aluminium transport in blood serum. Binding of aluminium by human transferrin in the presence of human albumin and citrate, Biochem. J. 280 (1991) 527–532.
[29] Z. Wei, J. Edin, A.E. Karlsson, K. Petrovic, I.L. Soroka, I. Odnevall Wallinder, Y. Hedberg, Can gamma irradiation during radiotherapy influence the metal release process for biomedical CoCrMo and 316L alloys? J. Biomed. Mater. Res. Part B Appl. Biomater. 106 (2018) 2673–2680.
[30] X. Wang, G. Herting, I. Odnevall Wallinder, E. Blomberg, Adsorption of bovine serum albumin on silver surfaces enhances the release of silver at pH neutral conditions, Phys. Chem. Chem. Phys. 17 (2015) 18524–18534.
[31] A. Larsen, M. Stoltenberg, G. Danscher, In vitro liberation of charged gold atoms: autometallographic tracing of gold ions released by macrophages grown on metallic gold surfaces, Histochem. Cell Biol. 128 (2007) 1–6.
[32] I. Milošev, From in vitro to retrieval studies of orthopedic implants, Corrosion 73 (2017) 1496–1509.
[33] J. Gilbert, Corrosion in the human body: metallic implants in the complex body environment, Corrosion 73 (2017) 1478–1495.
[34] Y. Okazaki, E. Gotoh, T. Manabe, K. Kobayashi, Comparison of metal concentrations in rat tibia tissues with various metallic implants, Biomaterials 25 (2004) 5913–5920.
[35] H. Agins, N. Alcock, M. Bansal, E. Salvati, P. Wilson, P. Pellicci, P. Bullough, Metallic wear in failed titanium-alloy total hip replacements, J. Bone Joint. Surg. 70 (1988) 347–356.
[36] Y. Okazaki, E. Gotoh, Comparison of metal release from various metallic biomaterials in vitro, Biomaterials 26 (2005) 11–21.
[37] J. Mariam, P. Dongre, D. Kothari, Study of interaction of silver nanoparticles with bovine serum albumin using fluorescence spectroscopy, J. Fluoresc. 21 (2011) 2193.
[38] X. Zhao, R. Liu, Y. Teng, X. Liu, The interaction between Ag+ and bovine serum albumin: a spectroscopic investigation, Sci. Total Env. 409 (2011) 892–897.